Society of Medical Education & Research

2025, Volume 5, Issue 1, Page No: 200-216
ISSN: 3108-4834

Archive of International Journal of Cancer and Allied Science

A Ruthenium-5-Fluorouracil Coordination Complex Induces Apoptosis and Autophagy While Suppressing Stemness in Colorectal Cancer Cells via Akt/mTOR Inhibition

Robert Ian Campbell[1]*, David Scott Wilson[1], Pieter Jan Verhoeven[2], Koen Maarten Peeters[2], Sarah Jane Collins[1]

[1]Department of Oncology, University of Glasgow, Glasgow, United Kingdom.
[2]Department of Cancer Biology, KU Leuven, Leuven, Belgium.

***E-mail** ✉ r.campbell.glasgow@gmail.com

Abstract

[Ru(5-FU)(PPh3)2(bipy)]PF6 (Ru/5-FU) is a newly developed ruthenium-based complex incorporating 5-fluorouracil, showing notable activity against colorectal cancer (CRC). In this study, we examined the molecular effects of Ru/5-FU in HCT116 CRC cells. Ru/5-FU demonstrated strong cytotoxic effects across multiple cancer cell types, including primary tumor cells, and triggered apoptosis in HCT116 cells. Treatment with Ru/5-FU lowered AKT1 mRNA levels and suppressed the expression of Akt1, phosphorylated Akt (pS473), and downstream effectors mTOR (pS2448), S6 (pS235/pS236), 4EBP1 (pT36/pT45), GSK-3β (pS9), and NF-κB p65 (pS529), without altering upstream regulators Hsp90 and PI3K p85/p55 (pT458/pT199), suggesting inhibition of Akt/mTOR signaling. Ru/5-FU also promoted LC3B accumulation and decreased p62/SQSTM1, indicating autophagy activation. Interestingly, blocking autophagy with 3-methyladenine or chloroquine enhanced Ru/5-FU cytotoxicity, suggesting autophagy has a protective role. Ru/5-FU reduced colony formation, decreased CD133+ populations, and impaired colonosphere formation, demonstrating suppression of cancer stem-like cells. Moreover, Ru/5-FU inhibited migration and invasion, coinciding with decreased vimentin and increased E-cadherin levels, pointing to disruption of epithelial-mesenchymal transition. In vivo, Ru/5-FU suppressed HCT116 tumor growth and lung metastasis in mouse xenografts. Collectively, these data indicate that Ru/5-FU may serve as an effective anti-CRC agent capable of targeting cancer stemness via Akt/mTOR inhibition.

Keywords: Colorectal cancer, Cancer cells, Tumorm, Migration, Lung metastasis

Introduction

Colorectal cancer (CRC) remains a significant global health issue, ranking third in incidence and second in cancer-related mortality. In 2020, CRC accounted for approximately 1.9 million new cases and 935,000 deaths worldwide [1]. The chemotherapeutic 5-fluorouracil (5-FU), first applied in 1957, continues to be a standard first-line treatment for advanced CRC, with response rates of 10–15%, which can increase to around 40–50% when combined with irinotecan or oxaliplatin [2, 3]. Targeted therapies are available for second-line management of metastatic CRC; however, mortality rates have remained relatively unchanged, emphasizing the need for novel treatments.

Modern cancer biology recognizes tumors as heterogeneous, containing small subpopulations called cancer stem cells (CSCs) capable of self-renewal and differentiation. CSCs contribute to tumor progression, recurrence, and therapy resistance [4-6]. Conventional chemotherapies often shrink tumors but enrich residual

Access this article online https://smerpub.com/

Received: 02 March 2025; **Accepted:** 05 June 2025

How to cite this article: Campbell RI, Wilson DS, Verhoeven PJ, Peeters KM, Collins SJ. A Ruthenium-5-Fluorouracil Coordination Complex Induces Apoptosis and Autophagy While Suppressing Stemness in Colorectal Cancer Cells via Akt/mTOR Inhibition. Arch Int J Cancer Allied Sci. 2025;5(1):200-16. https://doi.org/10.51847/iqrmviP98D

CSCs, promoting relapse [7-9]. Therefore, effective CRC therapy must eradicate CSCs to improve outcomes [4]. Recently, our team synthesized a novel ruthenium-5-FU complex, [Ru(5-FU)(PPh3)2(bipy)]PF6 (Ru/5-FU) **(Figure 1a)**, which exhibited higher efficacy than 5-FU in both 2D and 3D cultures and triggered caspase-mediated apoptosis in HCT116 cells [10]. This study investigates the molecular mechanisms of Ru/5-FU action, showing its ability to suppress CRC stemness through inhibition of Akt/mTOR signaling.

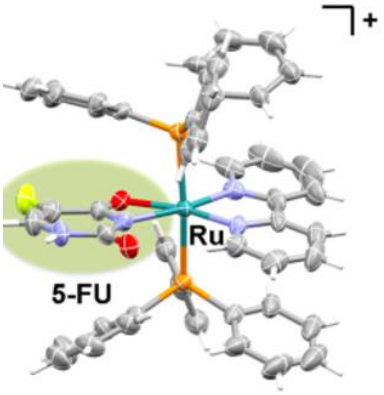

a)

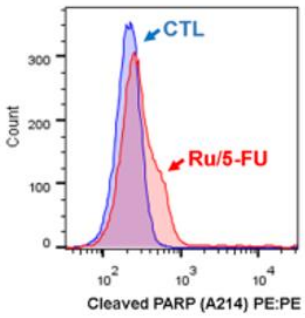

b)

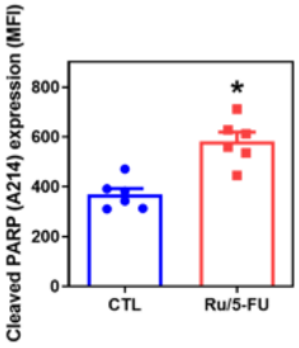

c)

Figure 1. Ru/5-FU induces apoptotic cell death. a) Chemical structure of Ru/5-FU. b, c)Flow cytometric analysis of PARP-1 levels in HCT116 cells following 24 h incubation with 4 µM Ru/5-FU. Vehicle (0.2% DMSO) served as control (CTL). Data represent mean ± S.E.M. of three independent experiments conducted in duplicate. * $P < 0.05$ versus CTL by Student's t test. MFI: Mean fluorescence intensity.

Materials and Methods

Ru/5-FU synthesis

Ru/5-FU was prepared and characterized following the procedure reported earlier [10]. All reagents were of analytical or reagent grade and obtained commercially from Sigma–Aldrich (Sigma–Aldrich, St. Louis, MO, United States) without further purification. Solvents were dried and distilled using conventional techniques. For biological assays, Ru/5-FU was prepared as a 5 mg/mL stock in sterile dimethyl sulfoxide (DMSO, Synth, Diadema, SP, Brazil) and subsequently diluted in culture medium to the desired concentrations.

Cell culture

This investigation employed a collection of 24 cancer cell lines, four primary cancerous cultures, two noncancerous cell lines, one primary noncancerous culture, and one mutant line alongside its parental counterpart. Cells were maintained according to supplier recommendations or standard ATCC protocols for mammalian cells. To ensure logarithmic growth, cultures were kept in flasks at 37°C under 5% CO2 atmosphere and passaged every 3-4 days. Adherent cultures were detached with 0.25% trypsin-EDTA solution (Sigma–Aldrich). Mycoplasma contamination was ruled out in all lines using a dedicated staining kit (Sigma–Aldrich). Cell viability was monitored throughout experiments via trypan blue exclusion, with initial cultures showing viability exceeding 90%.

Alamar blue assay

Cytotoxicity was determined using the Alamar blue method as outlined previously [11]. In brief, cells were plated in 96-well plates (7 × 103 cells/well for adherent types or 3 × 104 cells/well for suspension cultures). Following 24 h attachment, compounds were introduced and cells incubated for 72 h. Doxorubicin (Laboratory IMA S.A.I.C., Buenos Aires, Argentina) and 5-FU (Sigma–Aldrich) served as reference controls. Resazurin (30 µM; Sigma–Aldrich) was added at 20 µL per well either 4 h (cell lines) or 24 h (primary cells) prior to endpoint. Absorbance readings at 570 and 600 nm were

acquired on a SpectraMax 190 Microplate Reader (Molecular Devices, Sunnyvale, CA, USA).

Gene expression analysis

HCT116 cells were exposed to 4 µM Ru/5-FU for 12 h before total RNA extraction with the RNeasy Plus Mini Kit (Qiagen; Hilden, Germany) per protocol. RNA quality and quantity were assessed using a NanoDrop® 1000 spectrophotometer (Thermo Fisher Scientific, Waltham, Massachusetts, USA), followed by cDNA synthesis employing the Superscript VILO™ Kit (Invitrogen Corporation; Waltham, MA, USA). Gene profiling was conducted via qPCR on a TaqMan® array human cancer drug targets 96-well fast plate (ID RPRWENH, Applied Biosystems™, Foster City, CA, USA) using an ABI ViiA7 instrument (Applied Biosystems™). Thermal cycling included 2 min at 50 °C, 10 min at 95 °C, followed by 40 cycles of 15 s at 95 °C and 1 min at 60 °C. All steps were performed under RNase/DNase-free conditions. Relative mRNA levels were computed by the 2-ΔΔCT method [12] with Gene Expression Suite™ Software (Applied Biosystems™), using 0.2% DMSO-treated cells as calibrator. Normalization relied on the geometric mean of reference genes GAPDH, B2M, UBC, PGK1, RPLP0, and TRFC. Genes with RQ ≥ 2 were classified as upregulated (at least twofold increase versus control), while those with RQ ≤ 0.5 were deemed downregulated (at least 50% reduction versus control).

Flow cytometry assays

Expression of proteins was determined through flow cytometry with the use of fluorochrome-labeled primary antibodies. For intracellular targets, harvested cells underwent fixation in 4% formaldehyde (0.5–1 mL) for 10 min at 37 °C, followed by 1 min cooling on ice. Permeabilization involved gradual addition of precooled 100% methanol to chilled cells during mild vortexing, achieving 90% final concentration, and then 30 min on ice. Following rinses in incubation buffer (PBS plus 0.5% bovine serum albumin), antibodies were applied for 1 h incubation at room temperature. Post-PBS wash, fluorescence was recorded via flow cytometry.

For extracellular markers, cells received washes in incubation buffer (PBS supplemented with 0.5% bovine serum albumin), followed by 1 h antibody incubation at room temperature, PBS rinsing, and subsequent flow cytometric analysis of fluorescence. To identify CD133+ viable populations, YO-PRO-1 (Sigma–Aldrich) was employed for gating.

Functional evaluations of viability/apoptosis utilized annexin V-FITC/PI (FITC Annexin V Apoptosis Detection Kit I, BD Biosciences, San Jose, CA, USA) or YO-PRO-1/propidium iodide (PI) (Sigma–Aldrich). Inhibitors included: SP 600125 (JNK blocker, Cayman Chemical); PD 169316 (p38 MAPK blocker, Cayman Chemical); U-0126 (MEK blocker, Cayman Chemical); cyclic pifithrin-α (p53 blocker, Cayman Chemical); chloroquine (autophagy blocker, Ipca Laboratories, Mumbai, MH, India); 3-methyladenine (autophagy blocker, Sigma–Aldrich); and lithium chloride (Wnt pathway activator, Sigma–Aldrich).

Cell cycle progression and internucleosomal DNA breakdown were assessed via propidium iodide (PI) incorporation using a mixture of 0.1% Triton X-100, 2 µg/mL PI, 0.1% sodium citrate, and 100 µg/mL RNAse (all Sigma–Aldrich), incubated protected from light for 15 min at room temperature [13]. Cellular fluorescence was then measured by flow cytometry.

Data from all flow cytometry experiments were collected on a BD LSRFortessa analyzer with BD FACSDiva Software (BD Biosciences) and processed in FlowJo Software 10 (FlowJo Lcc; Ashland, OR, USA). Intracellular analyses involved at least 10,000 events per sample, while surface staining required a minimum of 30,000 events.

Phospho-specific ELISA

Levels of phosphorylated Histone H2AX (pS139) (catalog #DYC2288-2), JNK2 (pT183/Y185) (catalog #DYC2236-2), p38α (pT180/Y182) (catalog #DYC869B-2), and ERK1 (pT202/Y204) (catalog #DYC1825-2) were quantified in lysates via sandwich ELISA kits (R&D Systems, Inc., Minneapolis, MN, USA) per manufacturer guidelines. Cells were collected and lysed in buffer containing phosphatase/protease inhibitors plus 1 mM PMSF (all Sigma–Aldrich). Protein content was determined using Pierce Assay (Thermo Fisher Scientific, Waltham, MA, USA) against BSA standards. Optical density at 450 nm was read on a SpectraMax 190 Microplate Reader (Molecular Devices, Sunnyvale, CA, USA).

Transmission electron microscopy analyses

Samples were fixed for no less than 2 h in 0.1 M sodium cacodylate buffer (pH 7.4) with 2.5% glutaraldehyde and 2% paraformaldehyde. After washes, postfixation lasted 1 h in 1% osmium tetroxide, 0.8% potassium ferricyanide, and 5 mM calcium chloride. Dehydration

proceeded through graded acetone, followed by embedding in polybed epoxy resin. Thin sections received contrasting with 2% uranyl acetate and 2% lead citrate (aqueous) before viewing on a JEM-1230 electron microscope (JEOL, 1230, USA, Inc.).

Immunofluorescence

HCT116 cultures were grown on coverslips within 24-well plates and exposed to the compound for 24 h. Cells then underwent two saline rinses, 0.5% Triton X-100 permeabilization, 10 µg/mL RNAse treatment, and overnight incubation with fluorochrome-linked primary antibodies. Next day, PBS washes preceded mounting in Fluoromount-G plus DAPI (Invitrogen, Thermo Fisher Scientific). Confocal imaging was conducted using a Leica TCS SP8 system (Leica Microsystems, Wetzlar, HE, Germany).

Colony-forming assay

To evaluate clonogenicity, 1000 cells were placed in 6-well plates with 6 mL complete medium and subjected to the compound for 24, 48, or 72 h. Medium was then renewed without drug, and incubation continued to 14 days total. Fixation used methanol, staining employed 0.5% crystal violet, and colonies exceeding 50 cells were quantified via optical microscopy (Nikon, TS100).

Colonosphere assay

HCT116 cultures were maintained in serum-free DMEM-F12 medium enriched with 20 ng/mL EGF (PeproTech, USA), 20 ng/mL bFGF (PeproTech, USA), and B27 supplement (Invitrogen, Carlsbad, CA, USA) at a seeding density of 1.25 × 105 cells/mL in 24-well ultra-low attachment plates (Corning, USA). Treatments were applied at concentrations of 20, 10, 5, 2.5, and 1.25 µM. Sphere formation was documented by photographing at 0, 24, 48, and 72 h post-treatment using an inverted optical microscope (Leica, DMI8). Additionally, cells exposed to 4 µM Ru/5-FU were labeled with acridine orange (100 µg/ml) combined with PI (2 µg/ml) for confocal microscopy examination or with anti-CD133 antibody plus YO-PRO-1 for flow cytometric evaluation.

Wound healing assay

Migration assays were conducted based on established protocols [14] with minor adjustments. Cells were allowed to reach 80-90% confluence in 12-well plates before creating a scratch wound using a sterile plastic pipette tip. Detached cells and debris were removed by three saline washes, followed by incubation in serum-free medium containing the compound. Images of the wound front were captured at 0 and 72 h using an inverted optical microscope (Nikon, TS 100). Wound closure area was quantified employing ImageJ software (NIH, USA).

Transwell migration assay

Invasion capacity was evaluated in Transwell chambers following prior methods [15]. Cells were first starved in serum-free medium for 24 h. Inserts (8 µm pores; Corning, USA) in 6-well format were coated with Matrigel (Corning, USA). A suspension of 106 cells in 1.5 mL serum-free medium was placed in the upper compartment, while the lower compartment contained 2 mL medium supplemented with 20% FBS. After 48 h, non-invaded cells on the upper side were wiped away with cotton swabs. Invaded cells on the underside were fixed using 4% paraformaldehyde, stained with 0.5% crystal violet, imaged, and enumerated under an optical microscope (Leica, DMI8).

Animal models

Sixty-six female C. B-17 SCID mice (body weight 20-25 g) were obtained and maintained in pathogen-free housing at FIOCRUZ-BA facilities (Salvador, Bahia, Brazil) under an ethics-approved protocol (#10/2020). Animals had unrestricted access to standard chow and water in a controlled 12 h light/dark environment.

In the subcutaneous xenograft model, 107 HCT116 cells in 500 µL were injected into the left axillary region on day 0, as reported previously [16, 17]. Starting the next day, intraperitoneal administration (200 µL per animal) was performed daily for 14 days. Mice were divided into five randomized groups: group 1: vehicle (5% DMSO, n = 10); group 2: 5-FU 15 mg/kg (n = 10); group 3: DOX 0.8 mg/kg (n = 10); group 4: Ru/5-FU 2 mg/kg (n = 10); group 5: Ru/5-FU 4 mg/kg (n = 10). One day post-treatment cessation, euthanasia was performed via thiopental overdose (100 mg/kg), tumors were harvested, weighed, and prepared for histology. Tumor growth inhibition (%) was computed as [(A - B)/A] × 100, with A representing the mean tumor weight of the vehicle group and B that of the treated group.

For experimental pulmonary metastasis, 2 × 106 HCT116 cells in 100 µL were administered via the tail vein on day 0. Treatment began the following day via the intraperitoneal route (200 µL/animal) every alternate day for four weeks. Two randomized groups were established: group 1: vehicle (5% DMSO, n = 8); group

2: Ru/5-FU 4 mg/kg (n = 8). Euthanasia occurred one day after the final dose using thiopental overdose (100 mg/kg); lungs were removed, fixed in 4% formaldehyde, and metastatic nodules were counted before histological processing.

Throughout the studies, mice were observed for any signs of distress. Blood parameters were assessed on an Advia 60 analyzer (Bayer, Leverkusen, Germany). Major organs (liver, kidney, lung, heart) were excised, weighed, inspected macroscopically for alterations in color, lesions, or bleeding, and preserved in 4% formaldehyde. Tissues were sectioned with a blade, dehydrated in ethanol gradients, cleared in xylene, paraffin-embedded, sliced at 5 µm, stained with hematoxylin-eosin and/or periodic acid-Schiff (for liver/kidney), and evaluated microscopically.

Statistical analysis

Data are presented as means from ≥ three independent experiments (each in duplicate) ± S.E.M. or as IC50 with 95% confidence intervals. Comparisons between two groups employed a two-tailed unpaired Student's t-test, while multiple groups were analyzed by one-way ANOVA with Dunnett's post-hoc test using GraphPad Prism software (Intuitive Software for Science; San Diego, CA, USA).

Results and Discussion

Ru/5-FU exerts cytotoxicity in diverse cancer cell lines and induces apoptosis in HCT116 cells

Ru/5-FU showed cytotoxic effects in 24 cancer cell lines (HCT116, HepG2, NB4, THP-1, JUKART, K-562, HL-60, KG-1a, MDA-MB-231, MCF-7, 4T1, HSC-3, CAL 27, SCC-25, SCC4, SCC-9, A549, H1299, PANC-1, OVCAR-3, DU 145, U-87 MG, A-375, and B16-F10), with IC50 values ranging from 1.2 µM (OVCAR) to 9.2 µM (MCF-7), and 7.1, 8.9, and 3.1 µM for MRC-5, PBMC, and BJ noncancerous cells, respectively.

Doxorubicin (DOX) exhibited IC50 values from 0.03 µM (JUKART) to 18.6 µM (KG-1a) and 2.8, 1.3, and 0.7 µM in MRC-5, PBMC, and BJ cells, respectively. 5-FU showed IC50 values ranging from 5.2 µM (THP-1) to >192 µM (MCF-7 and HSC-3) and 31.3 µM (MRC-5) or >192 µM (PBMC, BJ).

Primary CRC cells, including cholangiocarcinoma and papilliferous malignant mesothelioma, treated with 25 µg/mL Ru/5-FU (27.4 µM) exhibited 70.1, 69.1, 81.2, and 78.4% reductions in viability, respectively. Comparable treatment with DOX (25 µg/mL; 46 µM) reduced viability by 71.0, 36.2, 65.6, 64.3%, and 5-FU (25 µg/mL; 192.2 µM) reduced viability by 4.1, 6.8, 54.8, 61.7%.

Given the activity against primary cells, we examined Ru/5-FU mechanisms in HCT116 cells. Ru/5-FU increased PARP cleavage (Asp214) **(Figures 1b and 1c)** and reduced BIRC5 and CDK5 expression **(Figure 2a)**, indicating apoptosis. Experiments using BAD KO SV40 MEF cells showed Ru/5-FU-induced cell death occurs independently of BAD.

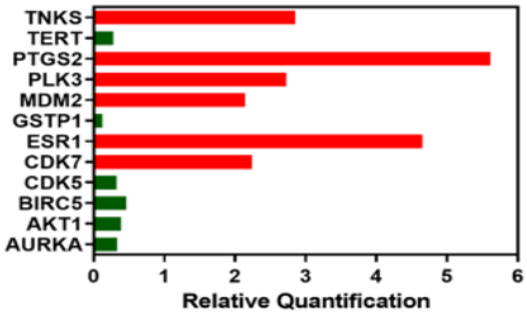

a)

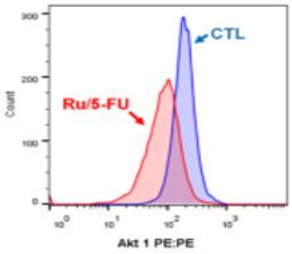

b)

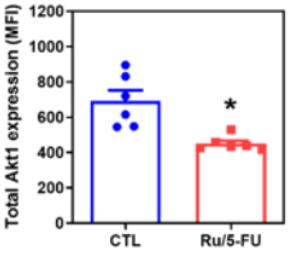

c)

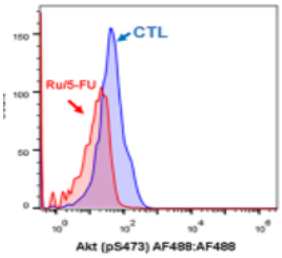

d)

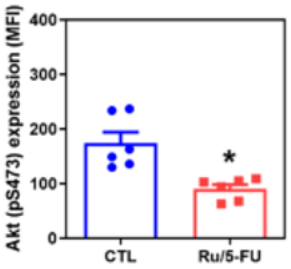
Akt (pS473) expression (MFI)
400
300
200
100
0
*
CTL
Ru/5-FU

e)

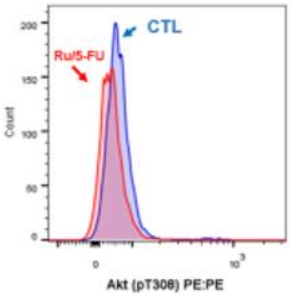
CTL
Ru/5-FU
Count
Akt (pT308) PE:PE

f)

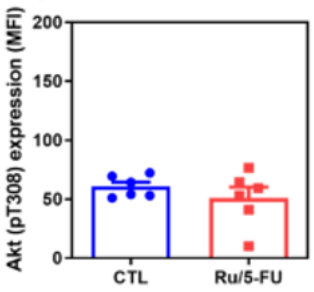
Akt (pT308) expression (MFI)
200
150
100
50
0
CTL
Ru/5-FU

g)

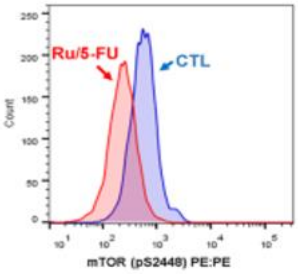
Ru/5-FU
CTL
Count
mTOR (pS2448) PE:PE

h)

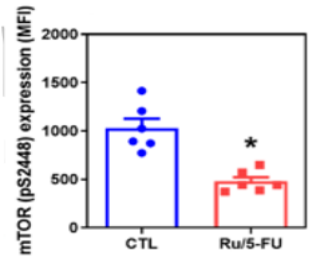
mTOR (pS2448) expression (MFI)
2000
1500
1000
500
0
*
CTL
Ru/5-FU

i)

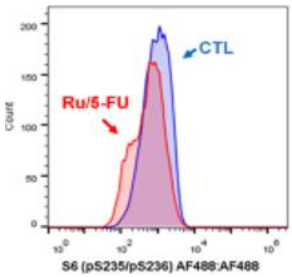
CTL
Ru/5-FU
Count
S6 (pS235/pS236) AF488:AF488

j)

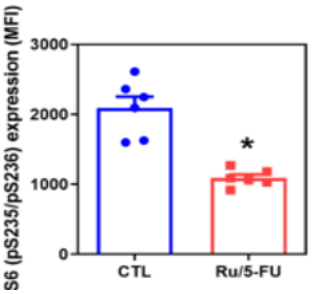
S6 (pS235/pS236) expression (MFI)
3000
2000
1000
0
*
CTL
Ru/5-FU

k)

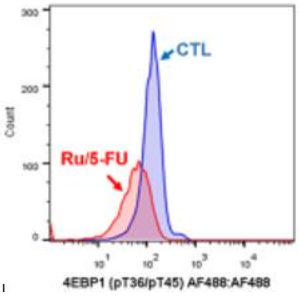
CTL
Ru/5-FU
Count
4EBP1 (pT36/pT45) AF488:AF488

l)

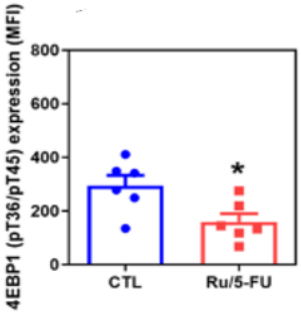
4EBP1 (pT36/pT45) expression (MFI)
800
600
400
200
0
*
CTL
Ru/5-FU

m)

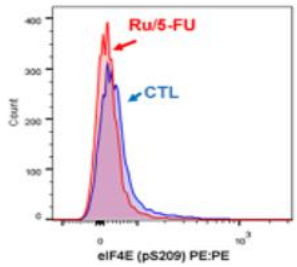
Ru/5-FU
CTL
Count
eIF4E (pS209) PE:PE

n)

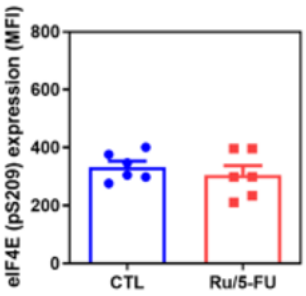

o)

Figure 2. Ru/5-FU inhibits the Akt/mTOR pathway. (a) Genes exhibiting up- or downregulation in HCT116 cells following 12 h exposure to 4 µM Ru/5-FU. Vehicle control consisted of 0.2% DMSO (CTL). Results are presented as relative quantification (RQ) relative to CTL. Genes were classified as upregulated when RQ ≥ 2 (red bars) and downregulated when RQ ≤ 0.5 (green bars). Flow cytometry-based quantification of Akt1 (b, c), Akt (pS473) (d, e), Akt (pT308) (f, g), mTOR (pS2448) (h, i), S6 (pS235/pS236) (J, K), 4EBP1 (pT36/pT45) (l, m), and eIF4E (pS209) (n, o) protein levels in HCT116 cells after 24 h treatment with 4 µM Ru/5-FU. Vehicle control was 0.2% DMSO (CTL). Values represent mean ± S.E.M. from three independent experiments performed in duplicate. *P < 0.05 versus CTL (Student's t test). MFI: Mean fluorescence intensity.

Ru/5-FU blocks Akt/mTOR signaling in HCT116 colorectal cancer cells

Using a qPCR array to screen 82 target genes, we detected significant downregulation of AKT1 (RQ = 0.392) in HCT116 cells treated with Ru/5-FU, pointing to Akt signaling as a key target of this compound **(Figure 2a)**. To validate this observation, we examined protein levels of Akt and related upstream/downstream components. Treatment with Ru/5-FU markedly reduced Akt1 and phosphorylated Akt (pS473) **(Figures 2b-2g).** Phosphorylation of downstream targets including mTOR (pS2448), S6 (pS235/pS236), and 4EBP1 (pT36/pT45) was also substantially lowered **(Figures 2h–2o).** In contrast, upstream regulators Hsp90 and phosphorylated PI3K p85/p55 (pT458/pT199) remained unaffected. Collectively, these data demonstrate selective inhibition of the Akt/mTOR axis by Ru/5-FU in HCT116 colorectal cancer cells.

Glycogen synthase kinase-3 (GSK-3) represents another downstream effector of Akt. Phosphorylation at Ser-9 on GSK-3β by Akt inactivates this kinase, which normally suppresses Wnt signaling. We observed decreased GSK-3β (pS9) levels in Ru/5-FU-treated HCT116 cells. This prompted us to test potential interference with Wnt activity; however, co-administration of lithium chloride (a Wnt pathway activator) failed to rescue cells from Ru/5-FU-induced death.

Akt additionally promotes NF-κB activation through Ikk-mediated degradation of IκB. We therefore evaluated effects on NF-κB signaling. While NF-κB p65 phosphorylation at S536 was unaltered **(Figures 3a and 3b),** phosphorylation at S529 was significantly reduced following Ru/5-FU exposure **(Figures 3c and 3d).** Furthermore, nuclear translocation of NF-κB p65 protein decreased in treated HCT116 cells, confirming disruption of NF-κB p65 activity **(Figure 3e)**. Doxorubicin (DOX), employed as a positive control NF-κB activator, elevated nuclear NF-κB p65 levels.

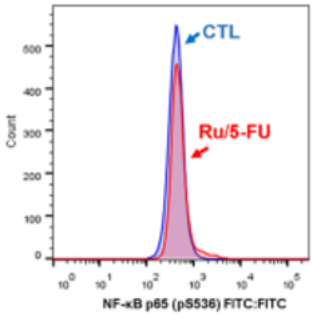

a)

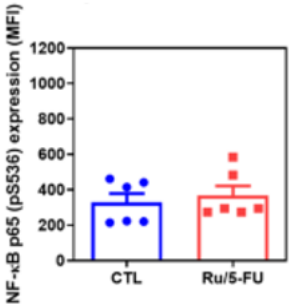

b)

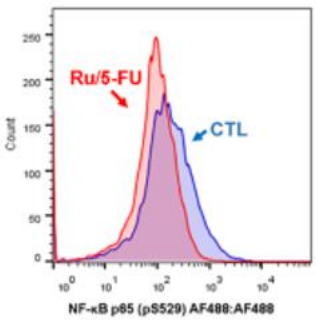

c)

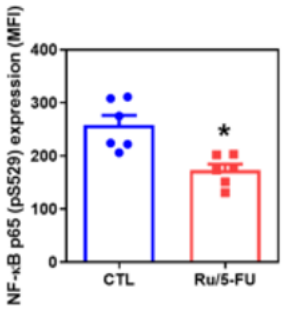

d)

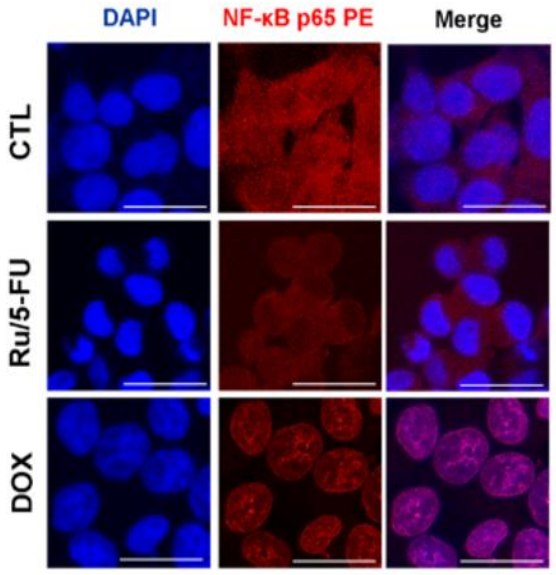

e)

Figure 3. Ru/5-FU impairs NF-κB pathway activation. Flow cytometric quantification of NF-κB p65 (pS536) (a, b) and NF-κB p65 (pS529) (c, d) in HCT116 cells after 24 h treatment with 4 µM Ru/5-FU. Vehicle control was 0.2% DMSO (CTL). Data represent mean ± S.E.M. from three independent experiments in duplicate. *P < 0.05 versus CTL (Student's t test). MFI: Mean fluorescence intensity. (e) Representative immunofluorescence staining for NF-κB p65 in HCT116 cells treated 24 h with 4 µM Ru/5-FU. Scale bar = 25 µm.

Akt enhances nuclear retention of Mdm2, thereby promoting p53 degradation. We thus explored possible activation of p53 by Ru/5-FU. Although the compound elevated the DNA damage indicator H2AX (pS139), no notable alterations in Mdm2 or phosphorylated p53 (pS15) were observed. Additionally, pharmacological p53 blockade using pifithrin-α did not attenuate Ru/5-FU-mediated cytotoxicity in HCT116 cells, supporting a p53-independent mechanism of cell death.

The epidermal growth factor receptor (EGFR) bridges Akt to the mitogen-activated protein kinase (MAPK) cascade. Accordingly, we explored if Ru/5-FU influences MAPK pathway activity. We evaluated phosphorylation status of key MAPK family members, including JNK2 (pT183/pY185), p38α (pT180/pY182), and ERK1 (pT202/pY204), in HCT116 colorectal cancer cells exposed to Ru/5-FU for brief periods (15 and 30 min) or longer duration (24 h). A transient rise in JNK2 (pT183/pY185) phosphorylation occurred at 15 min post-treatment. Nevertheless, adding inhibitors such as SP600125 (targeting JNK), PD169316 (targeting p38), or U-0126 (targeting MEK to prevent ERK1/2 phosphorylation) did not mitigate cytotoxicity caused by Ru/5-FU in HCT116 cells. This implies that activation of MAPK pathways plays no critical role in the mechanism of cell death triggered by Ru/5-FU.

Ru/5-FU activates autophagy in HCT116 colorectal cancer cells

Given that mTOR suppresses autophagy and Ru/5-FU lowers phosphorylated mTOR (pS2448) in HCT116 cells, we investigated potential stimulation of autophagic flux by this agent. We measured levels of autophagy markers LC3B and p62/SQSTM1 in cells subjected to Ru/5-FU. Exposure to the compound elevated LC3B **(Figures 4a, 4b and 3e**) and lowered p62/SQSTM1 **(Figures 4c, 4d and 4f),** supporting activation of autophagy. Moreover, transmission electron microscopy confirmed the accumulation of autophagic structures within treated HCT116 cells **(Figure 4g).**

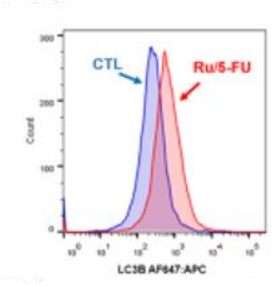

a)

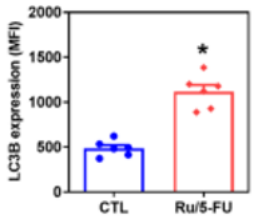

b)

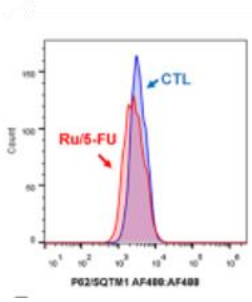

c)

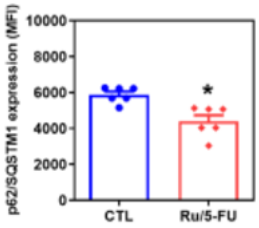

d)

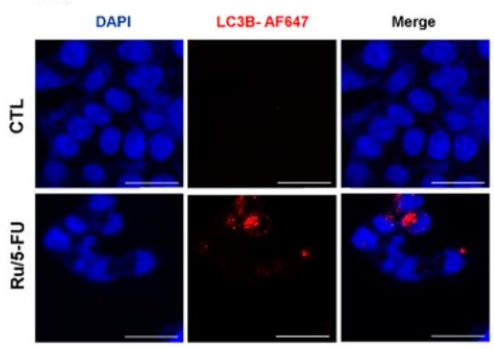

e)

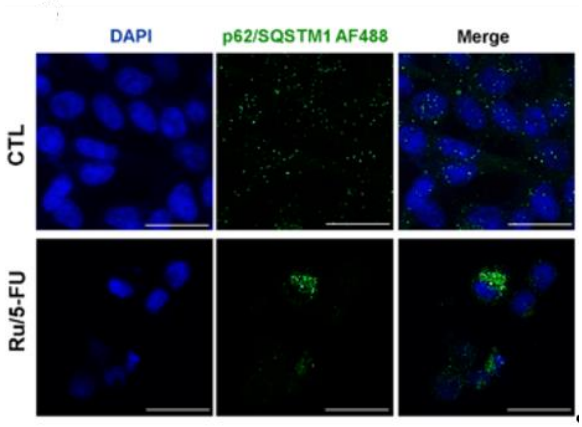

f)

Figure 4. Ru/5-FU stimulates autophagy. Assessment via flow cytometry of LC3B (a, b) and p62/SQSTM1 (c, d) levels in HCT116 cells following 24 h treatment with 4 µM Ru/5-FU. The control vehicle was 0.2% DMSO (CTL). Values denote mean ± S.E.M. derived from three separate experiments, each in duplicate. *P < 0.05 relative to CTL via Student's t test. MFI: Mean fluorescence intensity. (e) Typical immunofluorescence micrographs showing LC3B distribution in HCT116 cells after 24 h exposure to 4 µM Ru/5-FU. Scale bar = 25 µm. (f) Typical immunofluorescence micrographs showing p62/SQSTM1 distribution in HCT116 cells after 24 h exposure to 4 µM Ru/5-FU. Scale bar = 25 µm. (g) Typical transmission electron micrographs of HCT116 cells following 12 h treatment with 4 µM Ru/5-FU. Black asterisks mark vacant vacuoles, white asterisks mark dense mitochondria, and red asterisks mark autophagosomes. Scale bar = 2 µm.

Autophagy may serve protective or destructive functions during anticancer treatment. To define its contribution here, we applied pharmacological blockers of autophagy. We selected 3-methyladenine (3-MA), which interferes with initial autophagosome assembly through PI3K suppression, and chloroquine (CQ), which disrupts late-stage autophagosome-lysosome merging. Notably, 3-MA suppressed the elevation of LC3B prompted by Ru/5-FU. Each inhibitor amplified cytotoxicity from the compound, revealing that Ru/5-FU elicits a protective form of autophagy in HCT116 colorectal cancer cells.

Ru/5-FU attenuates cancer stem cell characteristics in HCT116 colorectal cancer cells

The Akt/mTOR and NF-κB axes are established drivers of colorectal cancer stem cell persistence. We thus assessed if Ru/5-FU disrupts stem-like features in HCT116 cells. Clonogenicity was tested over extended periods, revealing substantial dose- and duration-reliant declines in colony formation after Ru/5-FU exposure **(Figure 5a and 5b).** Furthermore, treatment diminished the fraction of CD133+ cells, recognized as a subpopulation enriched for colorectal cancer stem cells **(Figure 5c and 5d).**

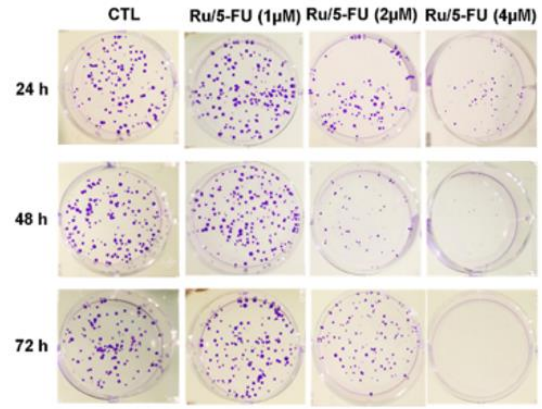

a)

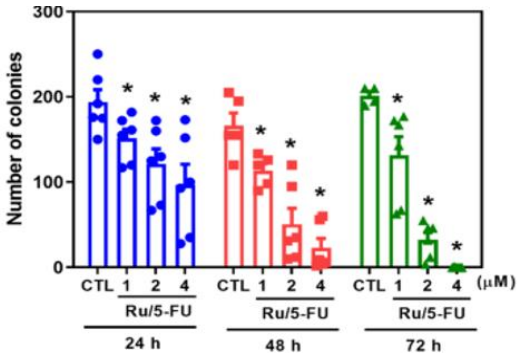

b)

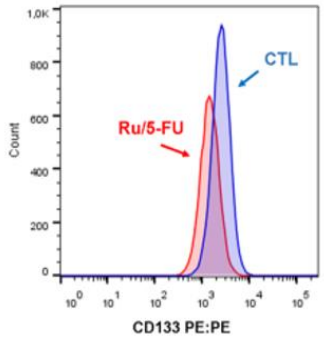

c)

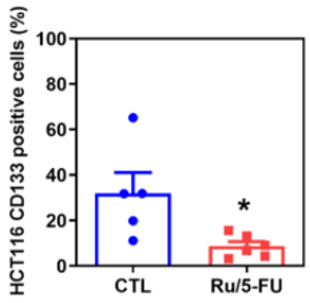

d)

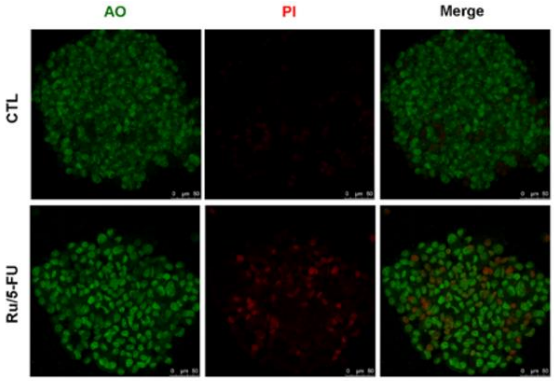

e)

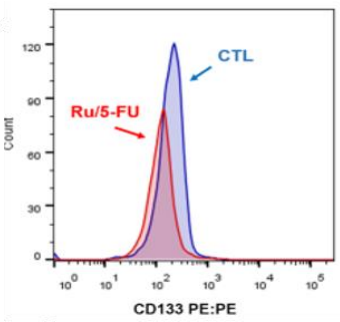

f)

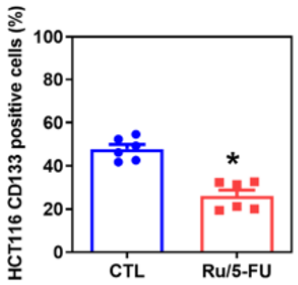

g)

Figure 5. Ru/5-FU targets colorectal cancer stem-like cells.

(a) Illustrative photographs and (b) measurement of colony counts derived from HCT116 cells following exposure to Ru/5-FU. (c, d) Evaluation of CD133 levels in HCT116 cells grown in monolayer culture after 24 h

treatment with 4 µM Ru/5-FU via flow cytometry. (e) Typical confocal micrographs of colonospheres generated from HCT116 cells post 24 h exposure to 4 µM Ru/5-FU. Staining involved acridine orange (AO, viable green cells) and propidium iodide (PI, necrotic red cells). Scale bar = 50 µm. (f, g) Measurement of CD133 levels in HCT116 colonosphere cultures after 24 h treatment with 4 µM Ru/5-FU via flow cytometry. Vehicle control was 0.2% DMSO (CTL). Results represent mean ± S.E.M. from three separate experiments, each in duplicate. *P < 0.05 versus CTL (Student's t test or one-way ANOVA with Dunnett's post-test).

We further examined the impacts of Ru/5-FU on HCT116-derived colonospheres. The compound similarly curtailed sphere generation in dose- and duration-reliant fashions, supporting its capacity to impair stem-like properties in HCT116 colorectal cancer cells. Elevated necrotic cell presence appeared in treated spheres **(Figure 5e**). Treated colonospheres additionally displayed fewer CD133+ HCT116 cells **(Figure 5f and 5g).**

Ru/5-FU blocks epithelial-mesenchymal transition in HCT116 colorectal cancer cells

Colorectal cancer stem-like populations exhibit traits resembling epithelial-mesenchymal transition (EMT), with shared regulation via pathways such as Akt/mTOR and NF-κB. We thus proposed that Ru/5-FU might counteract EMT in HCT116 cells. Initially, non-toxic doses of Ru/5-FU restricted cellular movement in scratch-wound assays **(Figures 6a and 6b**). Invasive potential was further probed using Matrigel-coated Transwell chambers mimicking extracellular matrix penetration, where Ru/5-FU likewise diminished invasion by HCT116 cells **(Figures 6c and 6d).**

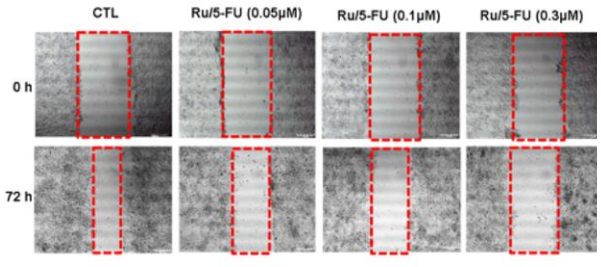

a)

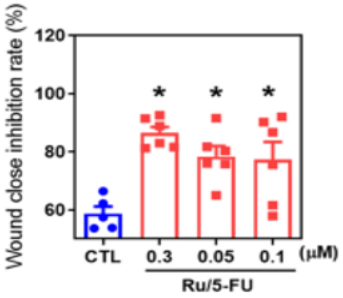

b)

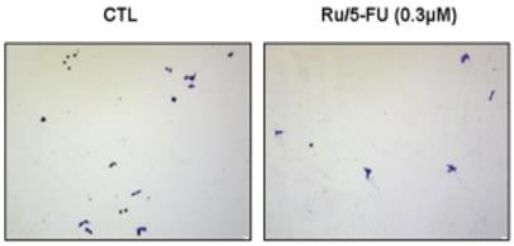

c)

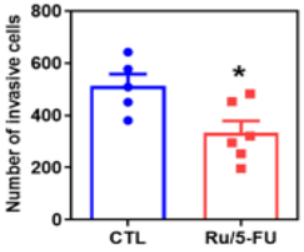

d)

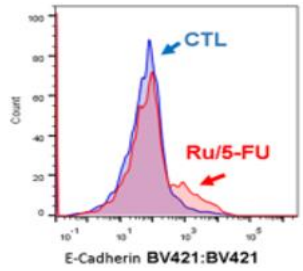

e)

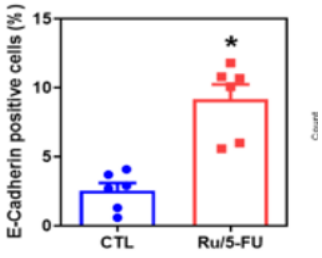

f)

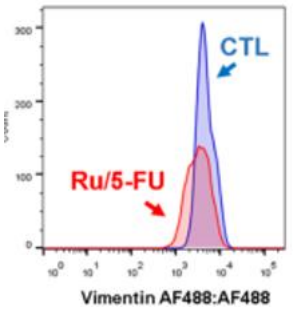

g)

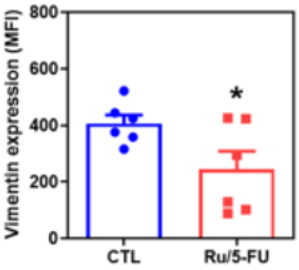

h)

Figure 6. Ru/5-FU restricts cellular migration and invasion.

(a) Illustrative photographs and (b) measurement of HCT116 migration in scratch assays after 72 h Ru/5-FU exposure. (c) Illustrative photographs and (d) measurement of HCT116 invasion in Transwell assays after 48 h Ru/5-FU exposure. Flow cytometric evaluation of E-cadherin (e, f) and vimentin (g, h) levels in HCT116 cells after 24 h treatment with 4 µM Ru/5-FU. Vehicle control was 0.2% DMSO (CTL). Results represent mean ± S.E.M. from three separate experiments, each in duplicate. *P < 0.05 versus CTL (Student's t test or one-way ANOVA with Dunnett's post-test). MFI: Mean fluorescence intensity.

Protein levels of key EMT indicators E-cadherin and vimentin were then measured in Ru/5-FU-exposed HCT116 colorectal cancer cells. E-cadherin amounts rose **(Figures 6e and 6f)**, whereas vimentin amounts fell **(Figures 6g and 6h)** upon treatment, confirming EMT interference by this agent in HCT116 cells.

Ru/5-FU curbs in vivo growth of HCT116 colorectal cancer cells and experimental pulmonary metastases in murine xenograft systems

In vivo actions of Ru/5-FU were explored across dual xenograft setups: one for primary tumor suppression and another for metastasis prevention. Antitumor efficacy was tested in C. B-17 SCID mice bearing subcutaneous HCT116 grafts. Mice received intraperitoneal Ru/5-FU at 2 or 4 mg/kg daily over two weeks **(Figure 7a).** Post-treatment, control tumors averaged 630.9 ± 46.8 mg. Ru/5-FU groups yielded averages of 595.5 ± 44.5 mg (low dose) and 419.0 ± 71.5 mg (high dose), equating to 5.6% and 33.6% growth restraint **(Figure 7b).** Half of the 5-FU-treated mice and one high-dose Ru/5-FU mouse perished during therapy. Positive controls doxorubicin (0.8 mg/kg) and 5-FU (15 mg/kg) achieved 25.4% and 47.9% reductions.

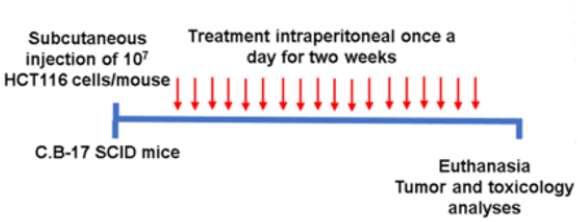

a)

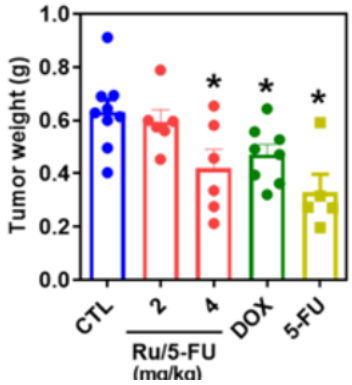

b)

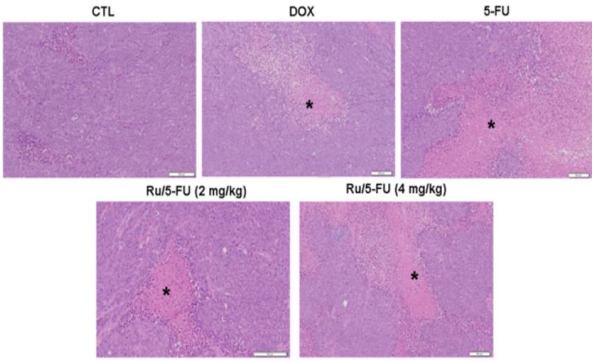

c)

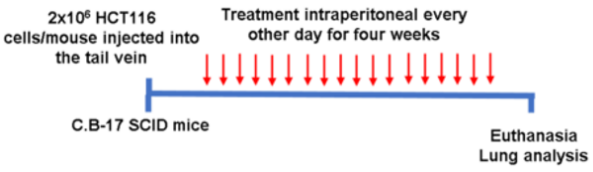

d)

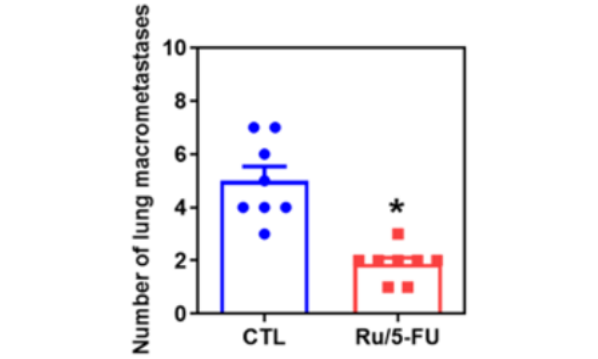

e)

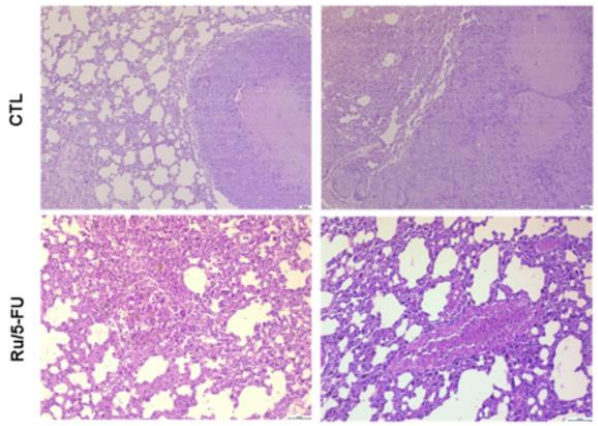

f)

Figure 7. Ru/5-FU demonstrates antitumor efficacy in murine models.

(a) Schematic of antitumor study design using Ru/5-FU in C. B-17 SCID mice with subcutaneous HCT116 implants. Daily intraperitoneal dosing at 2 and 4 mg/kg lasted two weeks. (b) Tumor growth suppression by Ru/5-FU. Vehicle was 5% DMSO (CTL). Doxorubicin (0.8 mg/kg) and 5-FU (15 mg/kg) served as references. Results represent mean ± S.E.M. (5–10 mice). (c) Typical hematoxylin-eosin stained HCT116 tumor sections viewed under light microscopy. Asterisks highlight necrotic zones. Scale bar = 100 µm. (d) Schematic of antimetastatic study design using Ru/5-FU in C. B-17 SCID mice with tail-vein HCT116 injection. Dosing at 4 mg/kg intraperitoneally occurred every other day for four weeks. (e) Metastasis suppression by Ru/5-FU. Vehicle was 5% DMSO (CTL). Results represent mean ± S.E.M. (8 mice). (f) Typical hematoxylin-eosin stained lung sections viewed under light microscopy. Scale bar = 50 or 100 µm. *P < 0.05 versus CTL (Student's t test or one-way ANOVA with Dunnett's post-test).

Histological examination of subcutaneous xenograft tumors revealed markedly anaplastic and highly mitotic malignant cells arranged in solid sheets with minimal stromal support **(Figure 7c).** Every tumor was graded as poorly differentiated adenocarcinoma. Although zones of coagulative necrosis accompanied by inflammatory infiltrates appeared across all treatment arms, these regions were substantially larger in mice receiving the maximum Ru/5-FU dose. By comparison, necrosis in vehicle-treated animals remained scattered and limited.

Antimetastatic efficacy of Ru/5-FU was evaluated in C. B-17 SCID mice following intravenous tail-vein delivery of HCT116 cells **(Figure 7d).** Mice received 4 mg/kg Ru/5-FU intraperitoneally on alternate days over four weeks. Pulmonary metastatic foci averaged 1.9 ± 0.2 in treated cohorts versus 5.0 ± 0.5 in vehicle controls **(Figure 7e**). Lung histology confirmed larger metastatic deposits (often with central necrosis) and higher nodule counts in untreated animals relative to the Ru/5-FU arm **(Figure 7f).**

Safety profiling was conducted in Ru/5-FU-treated mice. Significant body weight reduction occurred in groups exposed to 5-FU or the elevated Ru/5-FU dose ($p < 0.05$). Organ weights remained largely stable except for reduced liver mass in 5-FU recipients compared to controls. Hematologically, leukocyte counts were preserved in doxorubicin and low-dose Ru/5-FU groups but declined in 5-FU and high-dose Ru/5-FU animals. Erythrocyte numbers showed no meaningful variation across cohorts.

Organ histopathology (liver, kidney, lung, heart) was assessed via light microscopy. Liver tissue exhibited partial preservation amid moderate hydropic swelling and scattered coagulative hepatocyte necrosis. All groups displayed moderate vascular congestion plus focal mixed inflammatory infiltrates, with portal tracts ranging from intact to mildly disrupted. Kidney structure was maintained overall, though cortical tubular coagulative necrosis emerged focally in high-dose Ru/5-FU recipients; moderate congestion and minor glomerular hyalinization reducing urinary space appeared universally. Pulmonary architecture was partly conserved despite alveolar collapse (atelectasis) and septal thickening. Changes encompassed moderate-to-severe congestion, polymorph-dominant focal inflammation, mild fibrosis, plus localized hemorrhage and hemosiderin deposits. Metastatic deposits were restricted to the lungs in vehicle animals. Cardiac histology revealed no abnormalities in any cohort.

This investigation elucidates, for the first time, the mechanistic basis underlying the anticancer activity of the innovative ruthenium-5-fluorouracil conjugate Ru/5-FU. The agent demonstrated robust cytotoxic effects across diverse cancer lines and patient-derived primary cells representing multiple histologies. In HCT116 colorectal cancer cells, Ru/5-FU impaired stem-like traits primarily through blockade of Akt/mTOR signaling while promoting apoptosis. Additional outcomes included activation of protective autophagy and restraint of epithelial-mesenchymal transition. Within murine xenograft systems, Ru/5-FU effectively curtailed primary HCT116 tumor expansion and curtailed experimental pulmonary metastasis. A schematic overview of the proposed Ru/5-FU mechanism appears in **Figure 8**.

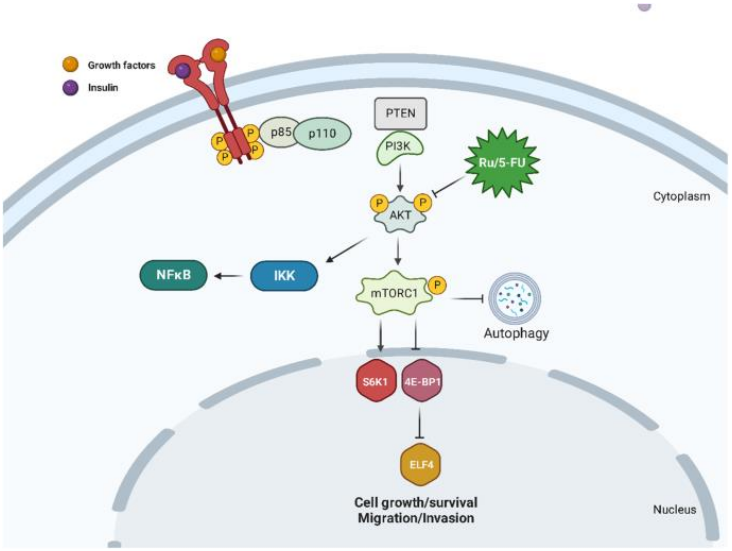

Figure 8. Schematic representation of the molecular pathways targeted by Ru/5-FU.

Prior work established that Ru/5-FU triggers apoptosis in HCT116 colorectal cancer cells [10]. Present findings reinforce this through marked elevation of cleaved PARP (Asp214) alongside diminished transcription of anti-apoptotic genes BIRC5 and CDK5 in treated cells. Apoptosis induction represents a recurring feature among varied ruthenium compounds targeting colorectal [16-18], leukemic [19, 20], hepatocellular [21-23], and mammary [24] malignancies.

Earlier reports indicated 5-FU-mediated S-phase arrest in HCT116 cultures; conversely, Ru/5-FU provoked DNA strand breaks without evident cell cycle phase accumulation, highlighting mechanistic divergence from parent 5-FU [10]. qPCR screening revealed AKT1 transcript suppression by Ru/5-FU. Protein analyses of PI3K/Akt/mTOR cascade components confirmed selective pathway inhibition extending to NF-κB. Additional transcript perturbations—downregulation of TERT (telomerase-related) and AURKA (mitotic regulator)—likely augment cytotoxicity. Despite reduced GSTP1 (antioxidant enzyme) expression, prior evidence excluded oxidative stress as a dominant contributor [10]. Cyclopentadienyl-ruthenium(II) derivatives reportedly trigger apoptosis in RKO and SW480 colorectal lines via MEK/ERK and PI3K/Akt suppression [25]. Cyclometalated ruthenium(II)-β-carboline agents elicited apoptosis in HeLa cells by attenuating ERK/Akt phosphorylation [26]. Isoquinoline-cyclometalated Ru(II) compounds promoted death in cisplatin-resistant A549 lung adenocarcinoma through Akt/GSK-3β/Fyn modulation [27]. A pyrimidine Schiff-base ruthenium(III) species induced HepG2 apoptosis concomitant with mTOR/Akt and NF-κB transcript reduction [28].

Certain ruthenium-piplartine conjugates drove MAPK-dependent (JNK/p38/ERK1/2), p53-reliant apoptosis in HCT116 cultures [15]. One Ru(II)-thymine derivative inflicted DNA lesions and p53-independent apoptosis in the same line [16]. Naphthalimide-bearing ruthenium(II) N-heterocyclic carbene complexes activated ROS-p38 MAPK signaling to cause HCT116 apoptosis [29]. In

contrast, Ru/5-FU-mediated lethality proceeded independently of both MAPK and p53 axes.

Ru/5-FU additionally modulated the levels of autophagy-related proteins LC3B and p62, likely through suppression of mTOR, a known inhibitor of autophagy. Autophagy exhibits a dual role in tumor development, potentially contributing to therapy resistance or promoting cell death [30-32]. In this work, cotreatment with autophagy blockers enhanced Ru/5-FU-triggered apoptosis, suggesting that the autophagy induced by Ru/5-FU exerts a protective effect in HCT116 cells. In a comparable manner, Ru(II) compounds combined with β-carboline alkaloids, when paired with autophagy blockers, promoted greater apoptosis in HeLa cells [33]. Within this framework, agents like chloroquine and hydroxychloroquine that inhibit autophagy are under evaluation in clinical studies to reverse resistance and increase tumor cell vulnerability to therapy [34, 35].

Ru/5-FU further reduced cancer stemness properties in HCT116 colorectal cancer cells, apparently via blockade of Akt/mTOR and NF-κB pathways, both established targets in cancer stem cells (CSCs). Notably, Ru(II)-p-cymene compounds derived from mesalazine also diminished stemness in HT-29 CRC cells [35]. Another Ru(II) triazine-based complex was shown to deplete CSCs in CD44+ subpopulations of HCT116 colorectal cancer and MCF-7 breast cancer cells [36].

Specifically, CSCs play a key role in cellular migration and invasion. Here, Ru/5-FU effectively impaired migration and invasion while altering the expression of EMT-associated markers E-cadherin and vimentin. A different ruthenium arene compound inhibited migration and invasion in A2780 ovarian cancer cells [37]. Additionally, ruthenium polypyridyl compounds decreased invasive behavior in A549 lung cancer cells [38].

The antitumor efficacy of Ru/5-FU in vivo was assessed using C. B-17 SCID mice bearing HCT116 xenografts. Remarkably, Ru/5-FU curtailed tumor progression and experimental pulmonary metastases with acceptable toxicity, despite lacking strong selectivity in vitro assays. Other Ru(II) compounds incorporating piplartine (15 μmol/kg/day) or a Ru(II)-thymine complex (1 and 2 mg/kg/day) similarly restricted tumor growth in HCT116-xenografted mice [6, 17]. A ruthenium arene complex bearing 1,10-phenanthroline-5,6-dione suppressed HCT116 cell proliferation in a zebrafish embryo model [39].

Conclusion

Overall, the findings suggest that Ru/5-FU represents a promising chemotherapeutic agent against colorectal cancer, capable of targeting and reducing stem-like features in CRC cells.

Acknowledgments: The authors are grateful to the flow cytometry, histotechnology and electron microscopy cores of FIOCRUZ-Bahia for collecting the flow cytometric data, performing the histological techniques and acquiring the MET and confocal microscopy data, respectively.

Conflict of Interest: None

Financial Support: This work received financial support and fellowships from the Brazilian agencies Coordenação de Aperfeiçoamento de Pessoal de Nível Superior (CAPES), Conselho Nacional de Desenvolvimento Científico e Tecnológico (CNPq), Fundação Oswaldo Cruz (Programa de Excelência em Pesquisa PROEP/IGM/2020 #IGM-002-FIO-20-2-6) and Fundação de Amparo à Pesquisa do Estado de São Paulo (FAPESP).

Ethics Statement: None

References

1. Sung H, Ferlay J, Siegel RL, Laversanne M, Soerjomataram I, Jemal A, et al. Global Cancer Statistics 2020: GLOBOCAN Estimates of Incidence and Mortality Worldwide for 36 Cancers in 185 Countries. CA Cancer J Clin. 2021;71:209–49.
2. Giacchetti S, Perpoint B, Zidani R, Le Bail N, Faggiuolo R, Focan C, et al. Phase III multicenter randomized trial of oxaliplatin added to chronomodulated fluorouracil-leucovorin as first-line treatment of metastatic colorectal cancer. J Clin Oncol. 2000;18:136–47.
3. Xie YH, Chen YX, Fang JY. Comprehensive review of targeted therapy for colorectal cancer. Signal Transduct Target Ther. 2020;5:22.
4. Silva VR, Santos LS, Dias RB, Quadros CA, Bezerra DP. Emerging agents that target signaling pathways to eradicate colorectal cancer stem cells. Cancer Commun (Lond). 2021;41:1275–313.

5. Frank MH, Wilson BJ, Gold JS, Frank NY. Clinical implications of colorectal cancer stem cells in the age of single-cell omics and targeted therapies. Gastroenterology. 2021;160:1947–60.
6. Ju F, Atyah MM, Horstmann N, Gul S, Vago R, Bruns CJ, et al. Characteristics of the cancer stem cell niche and therapeutic strategies. Stem Cell Res Ther. 2022;13:233.
7. Sprenger T, Conradi LC, Beissbarth T, Ermert H, Homayounfar K, Middel P, et al. Enrichment of CD133-expressing cells in rectal cancers treated with preoperative radiochemotherapy is an independent marker for metastasis and survival. Cancer. 2013;119:26–35.
8. Cho YH, Ro EJ, Yoon JS, Mizutani T, Kang DW, Park JC, et al. 5-FU promotes stemness of colorectal cancer via p53-mediated WNT/β-catenin pathway activation. Nat Commun. 2020;11:5321.
9. Chen L, Yang F, Chen S, Tai J. Mechanisms on chemotherapy resistance of colorectal cancer stem cells and research progress of reverse transformation: a mini-review. Front Med (Lausanne). 2022;9:995882.
10. Silva VR, Corrêa RS, Santos LS, Soares MBP, Batista AA, Bezerra DP. A ruthenium-based 5-fluorouracil complex with enhanced cytotoxicity and apoptosis induction action in HCT116 cells. Sci Rep. 2018;8:288.
11. Ahmed SA, Gogal RM Jr., Walsh JE. A new rapid and simple non-radioactive assay to monitor and determine the proliferation of lymphocytes: an alternative to [^{3}H]-thymidine incorporation assay. J. Immunol. Methods. 1994;170:211–24.
12. Livak KJ, Schmittgen TD. Analysis of relative gene expression data using real-time quantitative PCR and the 2(-Delta Delta C(T)) Method. Methods. 2001;25:402–8.
13. Nicoletti I, Migliorati G, Pagliacci MC, Grignani F, Riccardi C. A rapid and simple method for measuring thymocyte apoptosis by propidium iodide staining and flow cytometry. J Immunol Methods. 1991;139:271–9.
14. Burk RR. A factor from a transformed cell line that affects cell migration. Proc Natl Acad Sci USA. 1973;70:369–72.
15. Marshall J. Transwell(®) invasion assays. Methods Mol Biol. 2011;769:97–110.
16. Baliza IRS, Silva SLR, Santos LS, Neto JHA, Dias RB, Sales CBS, et al. Ruthenium complexes with piplartine cause apoptosis through MAPK signaling by a p53-dependent pathway in human colon carcinoma cells and inhibit tumor development in a xenograft model. Front Oncol. 2019;9:582.
17. Silva SLR, Baliza IRS, Dias RB, Sales CBS, Rocha CAG, Soares MBP, et al. Ru(II)-thymine complex causes DNA damage and apoptotic cell death in human colon carcinoma HCT116 cells mediated by JNK/p38/ERK1/2 via a p53-independent signaling. Sci Rep. 2019;9:11094.
18. Costa COS, Araujo Neto JH, Baliza IRS, Dias RB, Valverde LF, Vidal MTA, et al. Novel piplartine-containing ruthenium complexes: synthesis, cell growth inhibition, apoptosis induction and ROS production on HCT116 cells. Oncotarget. 2017;8:104367–92.
19. Oliveira MS, de Santana ÁAD, Correa RS, Soares MBP, Batista AA, Bezerra DP. Ru(II)-thymine complex causes cell growth inhibition and induction of caspase-mediated apoptosis in human promyelocytic leukemia HL-60 cells. Int J Mol Sci. 2018;19:1609.
20. Bomfim LM, de Araujo FA, Dias RB, Sales CBS, Rocha CAG, Correa RS, et al. Ruthenium(II) complexes with 6-methyl-2-thiouracil selectively reduce cell proliferation, cause DNA double-strand break and trigger caspase-mediated apoptosis through JNK/p38 pathways in human acute promyelocytic leukemia cells. Sci Rep. 2019;9:11483.
21. Carvalho NC, Neves SP, Dias RB, Valverde LF, Sales CBS, Rocha CAG, et al. A novel ruthenium complex with xanthoxylin induces S-phase arrest and causes ERK1/2-mediated apoptosis in HepG2 cells through a p53-independent pathway. Cell Death Dis. 2018;9:79.
22. Neves SP, de Carvalho NC, da Silva MM, Rodrigues ACBC, Bomfim LM, Dias RB, et al. Ruthenium complexes containing heterocyclic thioamidates trigger caspase-mediated apoptosis through MAPK signaling in human hepatocellular carcinoma cells. Front Oncol. 2019;9:562.
23. Lai Y, Lu N, Luo S, Wang H, Zhang P. A photoactivated sorafenib-ruthenium(II) prodrug for resistant hepatocellular carcinoma therapy through ferroptosis and purine metabolism disruption. J Med Chem. 2022;65:13041–51. https://doi.org/10.1021/acs.jmedchem.2c00880.

24. Graminha AE, Popolin C, Honorato de Araujo-Neto J, Correa RS, de Oliveira KM, Godoy LR, et al. New ruthenium complexes containing salicylic acid and derivatives induce triple-negative tumor cell death via the intrinsic apoptotic pathway. Eur J Med Chem. 2022;243:114772.
25. Teixeira-Guedes C, Brás AR, Teixeira RG, Valente A, Preto A. Ruthenium(II)-cyclopentadienyl-derived complexes as new emerging anti-colorectal cancer drugs. Pharmaceutics. 2022;14:1293.
26. Chen J, Deng Y, Wang J, Chen S, Peng F, He X, et al. Cyclometalated Ru(II) β-carboline complexes induce cell cycle arrest and apoptosis in human HeLa cervical cancer cells via suppressing ERK and Akt signaling. J Biol Inorg Chem. 2021;26:793–808.
27. Chen L, Wang J, Cai X, Chen S, Zhang J, Li B, et al. Cyclometalated Ru(II)-isoquinoline complexes overcome cisplatin resistance of A549/DDP cells by downregulation of Nrf2 via Akt/GSK-3β/Fyn pathway. Bioorg Chem. 2022;119:105516.
28. Noureldeen AFH, Aziz SW, Shouman SA, Mohamed MM, Attia YM, Ramadan RM, et al. Molecular design, spectroscopic, DFT, pharmacological, and molecular docking studies of novel ruthenium(iii)-schiff base complex: an inhibitor of progression in HepG2 Cells. Int J Environ Res Public Health. 2022;19:13624.
29. Dabiri Y, Schmid A, Theobald J, Blagojevic B, Streciwilk W, Ott I, et al. A ruthenium(II) N-heterocyclic carbene (NHC) complex with naphthalimide ligand triggers apoptosis in colorectal cancer cells via activating the ROS-p38 MAPK pathway. Int J Mol Sci. 2018;19:3964.
30. Shuhua W, Chenbo S, Yangyang L, Xiangqian G, Shuang H, Tangyue L, et al. Autophagy-related genes Raptor, Rictor, and Beclin1 expression and relationship with multidrug resistance in colorectal carcinoma. Hum Pathol. 2015;46:1752–9.
31. Galluzzi L, Vitale I, Aaronson SA, Abrams JM, Adam D, Agostinis P, et al. Molecular mechanisms of cell death: recommendations of the Nomenclature Committee on Cell Death 2018. Cell Death Differ. 2018;25:486–541.
32. Silva VR, Neves SP, Santos LS, Dias RB, Bezerra DP. Challenges and therapeutic opportunities of autophagy in cancer therapy. Cancers (Basel). 2020;12:3461.
33. Tan C, Lai S, Wu S, Hu S, Zhou L, Chen Y, et al. Nuclear permeable ruthenium(II) β-carboline complexes induce autophagy to antagonize mitochondrial-mediated apoptosis. J Med Chem. 2010;53:7613–24.
34. Ferreira PMP, Sousa RWR, Ferreira JRO, Militão GCG, Bezerra DP. Chloroquine and hydroxychloroquine in antitumor therapies based on autophagy-related mechanisms. Pharmacol Res. 2021;168:105582.
35. Acharya S, Ghosh S, Maji M, Parambil ARU, Singh S, Mukherjee A. Inhibition of 3D colon cancer stem cell spheroids by cytotoxic RuII-p-cymene complexes of mesalazine derivatives. Chem Commun (Camb). 2020;56:5421–4.
36. Purushothaman B, Arumugam P, Ju H, Kulsi G, Samson AAS, Song JM. Novel ruthenium(II) triazine complex [Ru(bdpta)(tpy)]2+ co-targeting drug resistant GRP78 and subcellular organelles in cancer stem cells. Eur J Med Chem. 2018;156:747–59.
37. Lv M, Qian X, Li S, Gong J, Wang Q, Qian Y, et al. Unlocking the potential of iridium and ruthenium arene complexes as anti-tumor and anti-metastasis chemotherapeutic agents. J Inorg Biochem. 2023;238:112057.
38. Jiang GB, Zhang WY, He M, Gu YY, Bai L, Wang YJ, et al. New ruthenium polypyridyl complexes functionalized with fluorine atom or furan: synthesis, DNA-binding, cytotoxicity and antitumor mechanism studies. Spectrochim Acta A: Mol Biomol Spectrosc. 2020;227:117534.
39. Lenis-Rojas OA, Roma-Rodrigues C, Carvalho B, Cabezas-Sainz P, Fernández Vila S, Sánchez L, et al. In vitro and in vivo biological activity of ruthenium 1,10-phenanthroline-5,6-dione arene complexes. Int J Mol Sci. 2022;23:13594.